Inorg. Chem. **2004**, *43*, 4137–4144

Synthesis, Structure, and Magnetic Properties of a Mn_{21} Single-Molecule Magnet

E. Carolina Sañudo,[†] Wolfgang Wernsdorfer,[‡] Khalil A. Abboud,[†] and George Christou*,[†]

Department of Chemistry and Center for X-ray Crystallography, University of Florida, Gainesville, Florida 32611-7200, and Laboratoire Louis Néel-CNRS, BP 166, 25 Avenue des Martyrs, 38042 Grenoble, Cedex 9, France

Received December 2, 2003

The reaction of $[Mn_3O(O_2CMe)_6(py)_3](ClO_4)$ (**1**; $3Mn^{III}$) with $[Mn_{10}O_4(OH)_2(O_2CMe)_8(hmp)_8](ClO_4)_4$ (**2**; $10Mn^{III}$) in MeCN affords the new mixed-valent complex $[Mn_{21}O_{14}(OH)_2(O_2CMe)_{16}(hmp)_8(pic)_2(py)(H_2O)](ClO_4)_4$ (**3**; $3Mn^{II}$–$18Mn^{III}$; hmp^- is the anion of 2-(hydroxymethyl)pyridine), with an average Mn oxidation state of +2.85. Complex **3**·7MeCN crystallizes in the triclinic space group $P\bar{1}$. The structure consists of a low symmetry $[Mn_{21}(\mu_4\text{-}O)_4(\mu_3\text{-}O)_{12}(\mu\text{-}O)_{16}]$ core, with peripheral ligation provided by 16 $MeCO_2^-$, 8 hmp^-, and 2 pic^- groups and one molecule each of water and pyridine. The magnetic properties of **3** were investigated by both dc and ac magnetic susceptibility measurements. Fitting of dc magnetization data collected in the 0.1–0.8 T and 1.8–4.0 K ranges gave $S = {}^{17}/_{2}$, $D \approx -0.086$ cm^{-1}, and $g \approx 1.8$, where S is the molecular spin of the Mn_{21} complex and D is the axial zero-field splitting parameter. ac susceptibility studies in the 10–997 Hz frequency range reveal the presence of a frequency-dependent out-of-phase ac magnetic susceptibility (χ_M'') signal consistent with slow magnetization relaxation rates. Fitting of dc magnetization decay versus time data to the Arrhenius equation gave a value of the effective barrier to relaxation (U_{eff}) of 13.2 K. Magnetization versus applied dc field sweeps exhibited hysteresis. Thus, complex **3** is a new member of the small but growing family of single-molecule magnets.

Introduction

Our group continues to have a strong interest in 3d metal carboxylate cluster chemistry. Employment of the appropriate types of ligands and reaction conditions has regularly allowed access to a variety of high nuclearity products with interesting structural, spectroscopic, and magnetic properties. Many of these have possessed large, and often abnormally large, numbers of unpaired electrons. This large spin (S), in combination with a sufficiently large magnetic anisotropy of the easy-axis (Ising) type, as reflected in a negative value of the axial zero-field splitting parameter (D), has led some of these species to be single-molecule magnets (SMMs). The latter are individual molecules that possess a sufficiently large barrier to magnetization relaxation to function as nanoscale magnets. Thus, an important goal in this field is the discovery of new examples of SMMs to improve our understanding of this interesting magnetic phenomenon. The family of SMMs has grown considerably over the past few years. Most of the new examples have been found in manganese chemistry, such as Mn_4,[1−3] Mn_{11},[4] Mn_{12},[5,6] Mn_{16},[7] Mn_{18},[8] Mn_{26},[9] and Mn_{30}.[10] SMMs with other metals have also been reported, such as Fe_4,[11] Fe_8,[11] Fe_{10},[12] and Fe_{19}[13] as well as V_4,[14] Co_4,[15] Ni_4,[16] Ni_{12},[17] and Ni_{21}[18] complexes.

* Author to whom correspondence should be addressed. E-mail: christou@chem.ufl.edu.
[†] University of Florida.
[‡] Laboratoire Louis Néel.

(1) Aubin, S. M. J.; Wemple, M. W.; Adams, D. M.; Tsai, H. L.; Christou, G.; Hendrickson, D. N. *J. Am. Chem. Soc.* **1996**, *118*, 7746.
(2) Yoo, J.; Brechin, E. K.; Yamaguchi, A.; Nakano, M.; Huffman, J. C.; Maniero, A. L.; Brunel, L. C.; Awaga, K.; Ishimoto, H.; Christou, G.; Hendrickson, D. N. *Inorg. Chem.* **2000**, *39*, 3615.
(3) Wernsdorfer, W., Aliaga-Alcalde, N., Hendrickson, D. N., Christou, G. *Nature* **2002**, *416*, 406.
(4) Eppley, H. J.; Aubin, S. M. J.; Wemple, M. W.; Adams, D. M.; Tsai, H. L.; Castro, S. L.; Sun, Z.; Folting, K.; Huffman, J. C.; Hendrickson, D. N.; Christou, G. *Mol. Cryst. Liq. Cryst. Sci. Technol., Sect. A* **1997**, *305*, 167.
(5) (a) Christou, G.; Gatteschi, D.; Hendrickson, D. N.; Sessoli, R. *MRS Bull.* **2000**, *25*, 67. (b) Sessoli, R.; Tsai, H. L.; Schake, A. R.; Wang, S.; Vincent, J. B.; Folting, K.; Gatteschi, D.; Christou, G.; Hendrickson, D. N. *J. Am. Chem. Soc.* **1993**, *115*, 1804. (c) Sessoli, R.; Gatteschi, D.; Caneschi, A.; Novak, M. A. *Nature* **1993**, *365*, 141. (d) Soler, M.; Chandra, S. K.; Ruiz, D.; Davidson, E. R.; Hendrickson, D. N.; Christou, G. *Chem. Commun.* **2000**, 2417−2418.
(6) Boskovic, C.; Brechin, E. K.; Streib, W. E.; Folting, K.; Bollinger, J. C.; Hendrickson, D. N.; Christou, G. *J. Am. Chem. Soc.* **2002**, *124*, 3725.
(7) Price, J. P.; Batten, S. R.; Moubaraki, B.; Murray, K. S. *Chem. Commun.* **2002**, 762.

10.1021/ic0353864 CCC: $27.50
Published on Web 04/08/2004

In our effort to find new examples of SMMs, new synthetic approaches are being developed. Soluble Mn(III) sources suitable for employment as starting materials for synthesis are not abundant. $Mn(O_2CMe)_3 \cdot 2H_2O$ is commercially available, but it is not very soluble in organic solvents; MnF_3 is also commercially available, but it introduces F^- ions into the reaction medium, which may also be a problem if the pH is acidic due to formation of HF. Our preferred sources for soluble Mn(III) reagents have been the trinuclear Mn(III) complexes of the general formula $[Mn_3O(O_2CR)_6(py)_3]ClO_4$ (R = Me, Et, or Ph). The reactivity of these complexes with a variety of chelating ligands has been studied by our group over many years,[19,8] and this approach has provided a rich source of new compounds. In addition, however, we have also employed as starting materials higher nuclearity clusters, which has often provided novel species not available from simpler reagents.

In the present work, we have employed an approach that is a hybrid of the above, namely, the reaction between preformed Mn_3 and Mn_{10} multinuclear complexes, in the belief that this might yield products that are not accessible from either complex individually. The chosen clusters both contain only Mn(III) ions, with the hope that this would facilitate the formation of Mn(III)-containing products. Indeed, this reaction has led to the formation and isolation of a novel Mn_{21} complex. We herein report the synthesis and characterization of $[Mn_{21}O_{14}(OH)_2(O_2CMe)_{16}(hmp)_8(pic)_2(py)(H_2O)](ClO_4)_4$ (**3**; hmp^- is the anion of 2-(hydroxymethyl)pyridine) obtained from the reaction of $[Mn_3O(O_2CMe)_6(py)_3](ClO_4)$ (**1**) with $[Mn_{10}O_4(OH)_2(O_2CMe)_8(hmp)_8](ClO_4)_4$ (**2**), and we show that this compound is a new addition to the growing family of SMMs.

Table 1. Crystallographic Data for Complex **3**·7MeCN

empirical formula	$C_{111}H_{132}Cl_4Mn_{21}N_{18}O_{77}$	α, deg	89.474(2)
formula weight	4245.89	β, deg	81.060(2)
temperature, K	73(2)	γ, deg	78.858(2)
crystal system	triclinic	volume, Å^3	8177.5(15)
space group	$P\bar{1}$	Z	2
a, Å	15.2067(17)	D_{calc}, g/cm^3	1.724
b, Å	16.7331(18)	R1[a,b]	0.0658
c, Å	33.165(4)	wR2[a,c]	0.1690

[a] 9416 unique data with $I > 2\sigma(I)$. [b] $R1 = \sum(||F_o| - |F_c||)/\sum|F_o|$. [c] $wR2 = [\sum[w(F_o^2 - F_c^2)^2]/\sum[w(F_o)^2]]^{1/2}$. $w = 1/[\sigma^2(F_o^2) + (mp)^2 + np]$. $p = [\max(F_o^2,0) + 2F_c^2]/3$ (m and n are constants). $\sigma = [\sum[w(F_o^2 - F_c^2)^2]/(n - p)]^{1/2}$.

Experimental Section

All materials were used as received. $[Mn_3O(O_2CMe)_6(py)_3]ClO_4$ (**1**)[20] and $[Mn_{10}O_4(OH)_2(O_2CMe)_8(hmp)_8](ClO_4)_4$ (**2**)[21] were prepared as reported; hmp^- is the anion of 2-(hydroxymethyl)pyridine.

$[Mn_{21}O_{14}(OH)_2(O_2CMe)_{16}(hmp)_8(pic)_2(py)(H_2O)](ClO_4)_4$ (3). To a solution of $[Mn_{10}O_4(OH)_2(O_2CMe)_8(hmp)_8](ClO_4)_4$ (**2**) (0.50 g, 0.21 mmol) in MeCN (50 mL) was added $[Mn_3O(O_2CMe)_6(py)_3]ClO_4$ (**1**) (0.54 g, 0.63 mmol). The solution was stirred overnight, filtered through Celite, and layered with Et_2O. After several weeks, the resulting dark red crystals of **3**·7MeCN were collected by filtration, washed with Et_2O, and dried in vacuo. Yield ~50%. Vacuum-dried crystals lose the MeCN solvent of crystallization and appear to be hygroscopic, being analyzed as the dihydrate. Anal. Calcd (Found) for **3**·$2H_2O$: C, 28.89 (29.15); H, 3.13 (2.95); N, 3.94 (3.86); Cl, 3.43 (3.55). Selected IR data in cm^{-1}: 1576 (vs), 1418 (s), 1089 (s), 1049 (m), 1018 (m), 760 (w), 712 (m), 663 (m), 625 (m), 597 (s). A sample for crystallography was kept in contact with the mother liquor to avoid solvent loss.

X-ray Crystallography. Data were collected at 173 K on a Siemens SMART platform equipped with a CCD area detector and a graphite monochromator utilizing Mo Kα radiation ($\lambda = 0.710\ 73$ Å). Cell parameters were refined using up to 8192 reflections. A full sphere of data (1850 frames) was collected using the ω-scan method (0.3° frame width). The first 50 frames were remeasured at the end of data collection to monitor instrument and crystal stability (maximum correction on I was <1%). An absorption correction by integration was applied on the basis of measured indexed crystal faces.

The structure of **3**·7MeCN was solved by direct methods in SHELXTL5[22] and refined using full-matrix least squares. The non-H atoms were treated anisotropically, whereas the H atoms were placed in calculated, ideal positions and were riding on their respective C atoms. The asymmetric unit consists of the complete $[Mn_{21}]^{4+}$ cation, four ClO_4^- anions, and seven MeCN molecules. The Mn(6) and Mn(7) centers were disordered along with their ligands. They were refined isotropically in two sites with their site occupation factors fixed at 50%. The four MeCN molecules were disordered and could not be modeled properly; thus, the program SQUEEZE,[23] a part of the PLATON[24] package of crystallographic

(8) Brechin, E. K.; Boskovic, C.; Wernsdorfer, W.; Yoo, J.; Yamaguchi, A.; Sañudo, E. C.; Concolino, T. R.; Rheingold, A. L.; Ishimoto, H.; Hendrickson, D. N.; Christou, G. *J. Am. Chem. Soc.* **2002**, *124*, 9710.
(9) Jones, L. F.; Brechin, E. K.; Collison, D.; Harrison, A.; Teat, S. J.; Wernsdorfer, W. *Chem. Commun.* **2002**, 2974.
(10) (a) Soler, M.; Rumberger, E.; Folting, K.; Hendrickson, D. N.; Christou, G. *Polyhedron* **2001**, *20*, 1365. (b) Soler, M.; Wernsdorfer, W.; Folting, K.; Pink, M.; Christou, G. *J. Am. Chem. Soc.* **2004**, *126*, 2156.
(11) (a) Gatteschi, D.; Sessoli, R.; Cornia, A. *Chem. Commun.* **2000**, 725. (b) Delfs, C.; Gatteschi, D.; Pardi, L.; Sessoli, R.; Wieghardt, K.; Hanke, D. *Inorg. Chem.* **1993**, *32*, 3099.
(12) Benelli, C.; Cano, J.; Journaux, Y.; Sessoli, R.; Solan, G. A.; Winpenny, R. E. P. *Inorg. Chem.* **2001**, *40*, 188.
(13) Goodwin, J. C.; Sessoli, R.; Gatteschi, D.; Wernsdorfer, W.; Powell, A. K.; Heath, S. L. *J. Chem. Soc., Dalton Trans.* **2000**, 1835.
(14) Sun, Z.; Grant, C. M.; Castro, S. L.; Hendrickson, D. N.; Christou, G. *Chem. Commun.* **1998**, 721.
(15) Yang, E.-Ch.; Hendrickson, D. N.; Wernsdorfer, W.; Nakano, M.; Zakharo, L. N.; Sommer, R. D.; Rheingold, A. L.; Ledezma-Gairaud, M.; Christou, G. *J. Appl. Phys.* **2002**, *91*, 7382.
(16) (a) Nakano, M.; Matsubayashi, G.-E.; Takaki, M.; Tatsuo, C. K.; Amaya, K.; Yoo, J.; Christou, G.; Hendrickson, D. N. *Mol. Cryst. Liq. Cryst. Sci. Technol., Sect. A* **2002**, *376*, 405. (b) Boskovic, C.; Rusanov, E.; Stoeckli-Evans, H.; Gudel, H. U. *Inorg. Chem. Commun.* **2002**, *5* (10), 881.
(17) (a) Cadiou, C.; Murrie, M.; Paulsen, C.; Villar, V.; Wernsdorfer, W.; Winpenny, R. E. P. *Chem Commun.* **2001**, 2666. (b) Andres, H.; Basler, R.; Blake, A. J.; Cadiou, C.; Chaboussant, G.; Grant, C. M.; Gudel, H.-U.; Murrie, M.; Simons, S.; Paulsen, C.; Semadini, F.; Villar, V.; Wernsdorfer, W.; Winpenny, R. E. P. *Chem.—Eur. J.* **2002**, *8*, 4867.
(18) Ochsenbein, S. T.; Murrie, M.; Rusanov, E.; Stoeckli-Evans, H.; Sekine, C.; Gudel, H. U. *Inorg. Chem.* **2002**, *41* (20), 5133.
(19) (a) Vincent, J. B.; Christmas, C.; Chang, H. R.; Li, Q.; Boyd, P. D. W.; Huffman, J. C.; Hendrickson, D. N.; Christou, G. *J. Am. Chem. Soc.* **1989**, *111*, 2086. (b) Schake, A. R.; Vincent, J. B.; Li, Q.; Boyd, P. D. W.; Folting, K.; Huffman, J. C.; Hendrickson, D. N.; Christou, G. *Inorg. Chem.* **1989**, *28*, 1915. (c) Libby, E.; McCusker, J. K.; Schmitt, E. A.; Folting, K.; Hendrickson, D. N.; Christou, G. *Inorg. Chem.* **1991**, *30*, 3486. (d) Sañudo, E. C.; Grillo, V. A.; Knapp, M. J.; Huffman, J. C.; Bollinger, J. C.; Hendrickson, D. N.; Christou, G. *Inorg. Chem.* **2002**, *41*, 2441.
(20) Vincent, J. B.; Chang, H. R.; Folting, K.; Huffman, J. C.; Christou, G.; Hendrickson, D. N. *J. Am. Chem. Soc.* **1987**, *109*, 5703.
(21) Aromi, G.; Aubin, S. M. J.; Bolcar, M. A.; Christou, G.; Eppley, H. J.; Folting, K.; Hendrickson, D. N.; Huffman, J. C.; Squire, R. C.; Tsai, H. L.; Wang, S.; Wemple, M. W. *Polyhedron* **1998**, *17*, 3005.

software, was used to calculate the solvent disorder area and remove its contribution to the overall intensity data. All four ClO_4^- anions were also disordered. A total of 1816 parameters were refined in the final cycle of refinement on F^2 using 42 653 reflections with $I > 2\sigma(I)$ to yield an R1 and a wR2 of 6.58 and 16.90%, respectively.

Other Studies. Infrared spectra (KBr disk) were recorded on a Nicolet NEXUS 670 spectrometer. Elemental analyses were performed by Atlantic Microlab, Inc., Norcross, GA. Variable-temperature magnetic susceptibility data were collected on powdered microcrystalline samples (restrained in eicosane to prevent torquing) with a Quantum Design MPMS-XL SQUID magnetometer equipped with a 7 T magnet. Pascal's constants were used to estimate the diamagnetic correction, which was subtracted from the experimental susceptibility to give the molar magnetic susceptibility (χ_M). Magnetization versus field hysteresis and direct current (dc) decay measurements at temperatures below 1.8 K were performed on single crystals, maintained in mother liquor, using a custom-made micro-SQUID instrument.

Results and Discussion

Synthesis. The reaction of $[Mn_{10}O_4(OH)_2(O_2CMe)_8(hmp)_8](ClO_4)_4$ (**2**) with $[Mn_3O(O_2CMe)_6(py)_3]ClO_4$ (**1**) in a 1:3 molar ratio in MeCN afforded a red solution. This was filtered and layered with diethyl ether, and from this, slowly grew dark red crystals of $[Mn_{21}O_{14}(OH)_2(O_2CMe)_{16}(hmp)_8(pic)_2(py)(H_2O)](ClO_4)_4 \cdot 7MeCN$ (**3**·7MeCN) in an isolated yield of 54%. The Mn_{21} cation is mixed-valent, with a 3Mn(II)−18Mn(III) oxidation state description. This allows rationalization of the unexpected presence of picolinate (pic^-, the anion of pyridine-2-carboxylic acid) groups in the product as being the result of the oxidation of hmp^- groups by Mn(III).[25] This is similar to the oxidation of $pdmH_2$ (pyridine-2,6-dimethanol) by Mn(III) observed recently in the formation of certain Mn_8 and Mn_9 products containing the oxidized, deprotonated form of $pdmH_2$ as a novel pentadentate chelate group.[26] The overall formation of **3** is summarized in eq 1; it is possible that some of the oxidizing equivalents required to convert the eight hmp^- groups to pic^- groups come from atmospheric oxygen, or from oxidation of solvent or ligand groups. Water is readily available in the solvent, which was not distilled.

$$\begin{aligned} 5[Mn_{10}O_4(OH)_2(O_2CMe)_8(hmp)_8]^{4+} + \\ 12[Mn_3O(O_2CMe)_6(py)_3]^{+} + 34H_2O \rightarrow \\ 4[Mn_{21}O_{14}(OH)_2(O_2CMe)_{16}(hmp)_8(pic)_2(py)(H_2O)]^{4+} + \\ 30pyH^{+} + 48MeCO_2H + 2py + 2Mn^{2+} + 18e^{-} \quad (1) \end{aligned}$$

Clearly, the formation of **3** must involve complicated fragmentation and aggregation steps, as well as redox chemistry. Thus, there are likely many Mn_x species in equilibrium in solution, and the exact species that preferentially crystallized (complex **3**) was dictated by relative solubilities, crystallization kinetics, and similar factors.

(22) Sheldrick, G. M. *SHELXTL5*; Bruker-AXS: Madison, WI, 1998.
(23) van der Sluis, P.; Spek, A. L. *Acta Crystallogr.* **1990**, *A46*, 194.
(24) Spek, A. L. *Acta Crystallogr.* **1990**, *A46*, 1.
(25) Kita, E.; Uscinska, G. *Transition Met. Chem.* **2003**, 373.
(26) Boskovic, C.; Wernsdorfer, W.; Folting, K.; Huffman, J. C.; Hendrickson, D. N.; Christou, G. *Inorg. Chem.* **2002**, *41*, 5107.

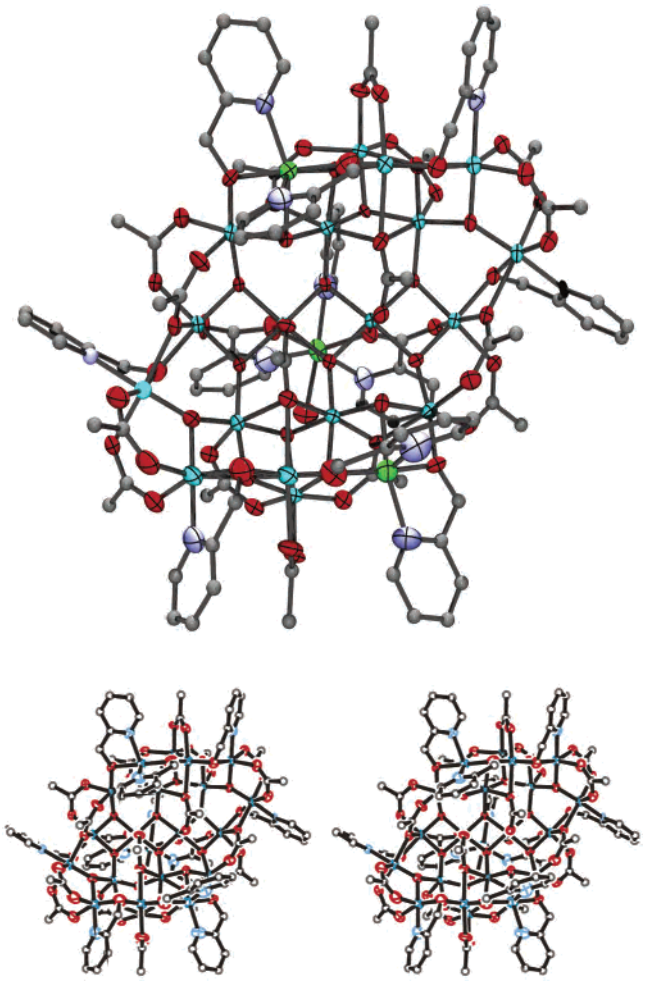

Figure 1. PovRay plot and stereoview at the 50% level of probability of the cation of complex **3**. The C atoms are shown as isotropic spheres for clarity.

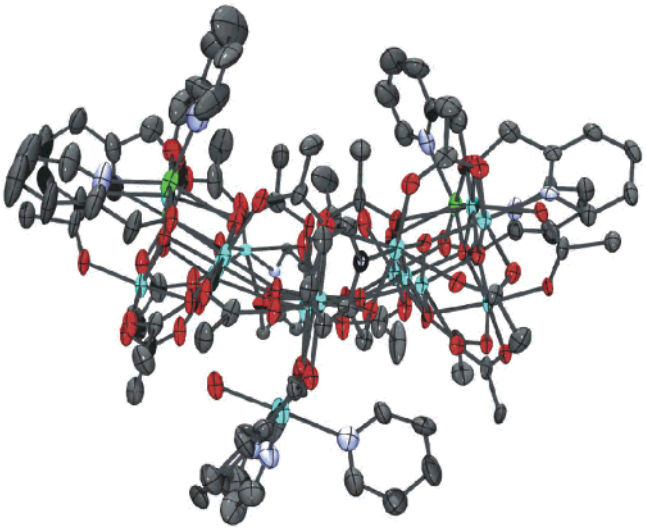

Figure 2. PovRay plot of a side view of the cation of complex **3**.

Description of the Crystal Structure. ORTEP representations of the cation of **3** and its Mn-oxide core are provided in Figures 1−3. Selected interatomic distances are listed in Table 2; full details are available as Supporting Information. Complex **3** crystallizes in the triclinic space group $P\bar{1}$. The asymmetric unit contains the complete Mn_{21} unit. This

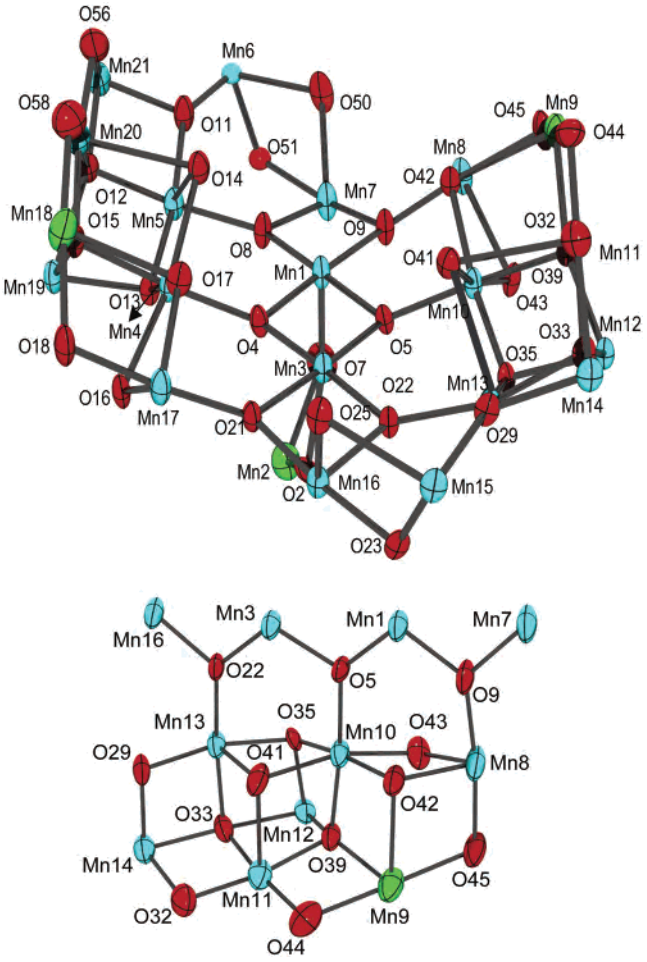

Figure 3. (top) Labeled PovRay plot of the core of the cation of complex **3** and (bottom) labeled detail of half of the core emphasizing the $[Mn_4O_4]$ cubane sharing faces with partial-cubanes.

Table 2. Average Interatomic Distances for the Cation of 3[a]

Mn···Mn	3.175	Mn(III)−O	1.916
Mn(II)−O	2.181	Mn(III)−O[b]	2.212
Mn(II)−N	2.189	Mn(III)−N	2.056

[a] In angstroms. A full listing of interatomic distances and angles is provided as Supporting Information. [b] O atoms on Mn(III) Jahn−Teller axes.

consists of a $[Mn_{21}(\mu_4\text{-}O)_4(\mu_3\text{-}O)_{10}(\mu_3\text{-}OH)_2(\mu\text{-}O)_{16}]$ core: The four μ_4-O (O(12), O(15), O(33), and O(39)) and ten μ_3-O atoms (O(4), O(5), O(8), O(9), O(11), O(13), O(21), O(22), O(29), and O(35)) are oxide ions. The two μ_3-OH^- groups are those at O(17) and O(42). Two of the μ-O atoms are from the two pic^- ligands (O(2) and O(7)), four are from η^1, η^2, and μ_3 acetate groups (O(14), O(16), O(25), O(41), O(43), and O(50)), and the remaining eight are from the hmp^- chelates (O(18), O(23), O(32), O(44), O(45), O(51), O(56), and O(58)). The core of **3** (Figure 3) is structurally related to that of the Mn_{18} complexes.[8] It contains the central, near-linear $[Mn_4O_6]$ unit (Mn(3), Mn(7), Mn(14), and Mn(19)), on each side of which there is a $[Mn_8O_{11}]$ unit. These two side units can be described as a central $[Mn_4O_4]$ cubane sharing two of its faces with two partial-cubanes (cubanes missing a vertex). One of the latter is sharing a face with a third partial-cubane, and the other is linked by one of its oxides, O(29), to a $[Mn_2O_2]$ unit that includes one of the Mn atoms in the central $[Mn_4O_6]$ unit (Mn(16) and Mn(7)). The resulting Mn_{20} molecule would be of virtual C_2 symmetry except that an additional Mn atom (Mn(2)) is linked by two pic^- anions to one end of the central $[Mn_4O_6]$ unit; this is best seen in the side view of Figure 2.

Table 3. Bond Valence Sums for Complex 3[a]

atom	Mn(II)	Mn(III)	Mn(IV)	atom	Mn(II)	Mn(III)	Mn(IV)
Mn(1)	3.269	**2.990**	3.139	Mn(12)	3.176	**2.905**	3.050
Mn(2)	**2.154**	2.029	2.035	Mn(13)	3.048	**2.788**	2.927
Mn(3)	3.182	**2.911**	3.056	Mn(14)	3.094	**2.859**	2.955
Mn(4)	3.205	**2.931**	3.078	Mn(15)	3.330	**3.079**	3.179
Mn(5)	3.207	**2.933**	3.079	Mn(16)	3.321	**3.038**	3.189
Mn(6)[b]	3.451	**3.185**	3.298	Mn(17)	3.213	**2.939**	3.086
Mn(7)[b]	3.519	**3.218**	3.379	Mn(18)	**2.167**	2.029	2.053
Mn(8)	3.250	**2.972**	3.120	Mn(19)	3.117	**2.851**	2.993
Mn(9)	**2.145**	2.005	2.034	Mn(20)	3.317	**3.034**	3.185
Mn(10)	3.213	**2.938**	3.085	Mn(21)	3.114	**2.879**	2.972
Mn(11)	3.230	**2.954**	3.101				

[a] The oxidation state for each metal is the whole number closest to the value in bold. [b] Average for the two disordered sites for O(51) and N(11).

Table 4. Bond Valence Sums for Oxygen Atoms in Complex **3**

atom	BVS	assignment	atom	BVS	assignment
O(1)	0.288	H_2O	O(17)	1.161	OH^-
O(4)	1.844	O^{2-}	O(21)	1.908	O^{2-}
O(5)	1.931	O^{2-}	O(22)	1.850	O^{2-}
O(8)	1.865	O^{2-}	O(29)	1.906	O^{2-}
O(9)	1.914	O^{2-}	O(33)	1.827	O^{2-}
O(11)	2.092	O^{2-}	O(35)	1.822	O^{2-}
O(12)	1.845	O^{2-}	O(39)	1.799	O^{2-}
O(13)	1.736	O^{2-}	O(42)	1.158	OH^-
O(15)	1.818	O^{2-}			

Close examination of the metric parameters, detection of Mn(III) Jahn−Teller (JT) elongation axes, and bond valence sum (BVS) calculations[27] indicate the trapped-valence $[Mn(II)_3Mn(III)_{18}]$ oxidation state description for the complex. Two of the Mn(II) atoms are part of two of the side units, Mn(9) and Mn(18), and the third one is the unique Mn(2) unit. The latter is also bound to a terminal pyridine and a water molecule, O(1). Four ClO_4^- counterions are seen in the crystal structure, confirmed by Cl analysis (see the Experimental Section). Charge balance requires the presence of two additional protons beyond those attached to the C atoms or in the H_2O group. Their positions were identified by BVS calculations on O atoms.[28,29] Those in the hmp groups had BVS values >1.7, confirming them as deprotonated, which is as expected from their bridging modes. The BVS values for the oxide O atoms, however, (Table 4) identified two of them as having BVS values of ∼1, indicating them to be monoprotonated, that is, OH^- groups. These are O(17) and O(42), as already mentioned above. They participate in intramolecular hydrogen bonds with adjacent acetate O atoms (O(17)···O(3) = 2.692 Å and O(42)···O(6) = 2.633 Å), and this no doubt stabilizes the protonation of what would otherwise be μ_3-O^{2-} ions, the usually preferred situation for triply bridging O atoms between Mn(II) and 2Mn(III).

(27) Liu, W.; Thorp, H. H. *Inorg. Chem.* **1993**, *32*, 4102.
(28) Brown, I. D., Shannon, R. D. *Acta Crystallogr.* **1973**, *A29*, 266.
(29) Donnay, G.; Allman, R. *Am. Mineral.* **1970**, *55*, 1003.

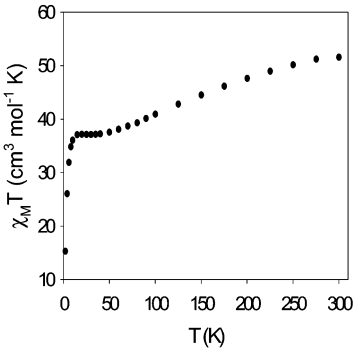

Figure 4. dc magnetic susceptibility of **3** in the 5.0−300 K range in a 1.0 T applied field.

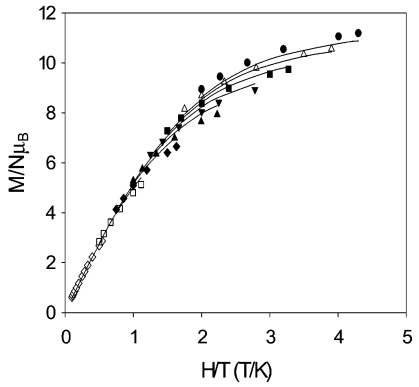

Figure 5. Plots of reduced magnetization ($M/N\mu_B$) vs H/T for **3** in applied dc fields of 0.1 (◇), 0.2 (□), 0.3 (◆), 0.4 (▲), 0.5 (▼), 0.6 (■), 0.7 (△), and 0.8 (●) T and in the 1.8−4.0 K range. The solid lines are the fits of the data; see the text for the fitting parameters.

Each Mn(III) atom in an octahedral coordination environment will display a Jahn−Teller distortion.[30] This distortion is usually an axial elongation, and this is what is observed in complex **3**. In addition, the JT axes of the central [Mn_4O_6] unit are all aligned parallel, and those of the other Mn(III) atoms are nearly parallel to these, except for those of Mn(6), Mn(11), Mn(15), and Mn(20), which have their JT elongation axes nearly perpendicular to the rest. This point will be of particular importance to the magnetic properties of **3** (see below), because the orientation of the Mn(III) JT axes is the main factor that determines the overall magnetic anisotropy of the molecule.

At first glance, Mn(5) and Mn(13) appear to be pentacoordinated, with square pyramidal geometry and the Mn atom in the base of the pyramid. Closer examination, however, reveals an elongated Mn−O contact in what would be the sixth coordination site of highly distorted octahedral coordination; Mn(5)−O(14) is 2.502 Å, and Mn(13)−O(34) is 2.544 Å. These long bonds are trans to the elongated Mn(5)−O(10) and Mn(13)−O(34) bonds (2.145 and 2.160 Å, respectively). These contacts are long but undoubtedly real, and Mn(5) and Mn(13) are best considered octahedrally coordinated with a very large JT elongation along the O(10)−Mn(5)−O(14) and O(34)−Mn(13)−O(22) axes.

Finally, there are few intermolecular interactions between separate Mn_{21} units. The only significant such interactions are π-stacking contacts involving the aromatic rings of some hmp^- ligands at an average distance of 3.6 Å.

Magnetic Susceptibility Studies. The solid state dc magnetic susceptibility of a microcrystalline sample of **3**·$2H_2O$ (restrained in eicosane to avoid torquing) is shown as a $\chi_M T$ versus T plot in Figure 4. The $\chi_M T$ value decreases with decreasing temperature from 51.5 cm^3 K mol^{-1} at 300 K to a plateau at 37.1 cm^3 K mol^{-1} between 50 and 15 K, and then it sharply drops to 16.0 cm^3 K mol^{-1} at 4.0 K. The plateau region suggests a large ground state spin (S) value for the complex, with the sharp decrease at the lowest temperatures due to Zeeman effects. The plateau value is consistent with an $S = {}^{17}/_2$ ground state and a g value slightly less than 2.0, as expected for Mn(III). The spin-only ($g = 2$) value for an $S = {}^{17}/_2$ state is 40.38 cm^3 K mol^{-1}.

It is clearly not possible, due to the great size and complexity of the Mn_{21} magnetic system, to readily determine by matrix diagonalization the individual Mn_2 pairwise exchange interactions in the molecule[31] nor is it possible to apply an equivalent operator approach based on the Kambe vector coupling method.[32] We thus concentrated instead on identifying the ground state S value of the complex. The latter for a 3Mn(II)−18Mn(III) system can in theory take any value from ${}^1/_2$ to ${}^{87}/_2$. With such a large spin system and the presence of Mn(II) ions, which are known to give weak exchange interactions, it was anticipated that there might be a high density of low-lying excited states. Additionally, since the exchange interactions are expected to be mostly antiferromagnetic in nature, some of the lower-lying excited states are likely to have S values larger than that of the ground state.

The method used to determine the ground state S value of the cluster was the fitting of variable-temperature and -field magnetization (M) data collected on a polycrystalline sample in the 1.8−4.0 K temperature range and 0.1−0.8 T applied dc field range. Small values of the latter were employed to avoid problems from any low-lying excited states with S values greater than that of the ground state, whose M_S components would approach and cross those of the ground state in big enough applied fields. The obtained magnetization (M) data are plotted as reduced magnetization ($M/N\mu_B$) versus H/T in Figure 5. They were fit to a model that assumes only the ground state is populated, includes axial zero-field splitting ($D\hat{S}_z^2$) and the Zeeman interaction, and incorporates a full powder average.

To calculate the magnetization for a polycrystalline powder sample, a suitable averaging of the magnetization must be carried out. In the case of low magnetic fields and high temperatures, where M is a linear function of field H, this entails simply numerically averaging the three principal values M_x, M_y, and M_z. In the region of high fields and low temperatures, a true powder-average of M for all orientations must be made[33] using eq 2.

(30) Cotton, F. A.; Wilkinson, G. *Advanced Inorganic Chemistry*, 4th ed.; John Wiley and Sons: New York, 1980.

(31) Kahn, O. *Molecular Magnetism*; Verlag Chemie: New York, 1993.
(32) Kambe, K. *J. Phys. Soc. Jpn.* **1950**, *5*, 48.

$$\bar{M} = \frac{-N}{4\pi}\int_{\theta=0}^{\pi}\int_{\phi=0}^{2\pi}\left[\sum_i\left(\frac{\delta E_i}{\delta H}\right)\times \exp(-E_i/kT)/\sum_i \exp(-E_i/kT)\right]\sin\theta\, d\theta\, d\phi \quad (2)$$

In this equation, θ and ϕ are the polar angle orientations of the field with respect to the molecular principal axis system, N is Avogadro's number, and $\delta E_i/\delta H$ is the change in the energy of the ith level in response to a change in a magnetic field. The energies of the various spin sublevels of the ground state S are obtained by diagonalization of the $(2S + 1)(2S + 1)$ spin Hamiltonian matrix, including the Zeeman terms, and the derivatives of the energy with respect to the magnetic field are calculated from the corresponding eigenvectors by using the Hellmann−Feynman theorem.[33] For complexes with no zero-field splitting, the plot of M versus H follows a simple Brillouin function, where the M saturates at a value of gS and the isofield lines are superimposed.

The program MAGNET[34] was employed to fit the experimental data to those calculated using the above procedure for different values of S, D, and g. The best fits are shown as the solid lines in Figure 7, and the fit parameters were $S = {}^{17}/_{2}$, $D \approx -0.086$ cm^{-1}, and $g \approx 1.8$. The S value is thus the same as suggested from the plateau of Figure 4. However, the D value is likely only an approximation, given the assumptions made (such as that the molecule has axial symmetry) and the only fair quality of the fit.

Such a large S value, together with a negative D value, suggested that **3** might exhibit the slow magnetization relaxation rate of a SMM. The upper limit for the relaxation barrier for a half-integer spin system is given by $(S^2 - {}^1/_4)|D|$, and the very small absolute D value unfortunately suggests only a small barrier. Nevertheless, it might still be large enough to give magnetization hysteresis, the classical and diagnostic property of a magnet, and this was therefore explored by alternating current (ac) magnetic susceptibility studies.

In an ac magnetic susceptibility experiment, a weak magnetic field (typically in the 1−5 G range) oscillating at some ac frequency is applied to a sample to investigate its magnetization relaxation dynamics. If the magnetization vector can relax fast enough to keep up with the oscillating field, then there is no imaginary (out-of-phase) susceptibility signal (χ_M''), and the real (in-phase) susceptibility (χ_M') is equal to the dc susceptibility. If the barrier to magnetization relaxation is significant compared to thermal energy (kT), however, then there is a nonzero χ_M'' signal and the in-phase signal decreases. In addition, the χ_M'' signal is frequency-dependent. Such frequency-dependent χ_M'' signals are a characteristic signature of the superparamagnetic-like properties of a SMM (but by themselves do not prove the presence of a SMM). Thus, ac magnetic susceptibility data for a microcrystalline sample of complex **3**·2H$_2$O were collected in the 1.8−6.0 K range at several frequencies in the 10−997 Hz range, and they are plotted as χ_M'' and $\chi_M'T$ in Figure 6. A frequency-dependent decrease in the $\chi_M'T$ signal was indeed observed at temperatures below 2.5 K, together with a corresponding appearance of a frequency-dependent χ_M'' signal, but the maxima to the latter signals clearly occur at temperatures below the 1.8 K operating limit of our SQUID instrument.

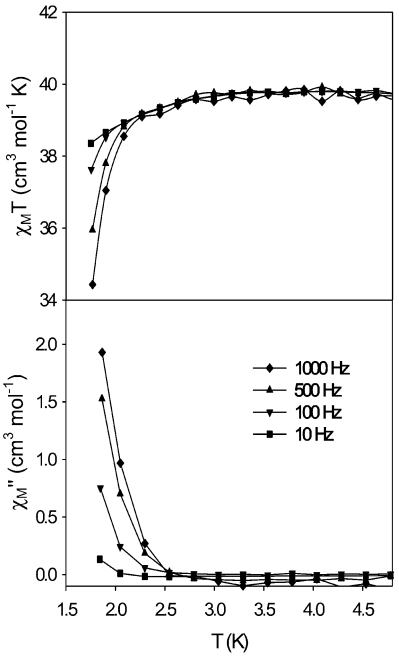

Figure 6. ac magnetic susceptibility of **3** at the indicated ac oscillation frequencies: (top) the in-phase (χ_M') signal, plotted as $\chi_M'T$; (bottom) the out-of-phase (χ_M'') signal.

The $\chi_M'T$ value at temperatures above 3 K is essentially constant at just under 40 cm^3 K mol^{-1}, and this can be used to calculate the ground state spin of the molecule. In the absence of a χ_M'' signal, the $\chi_M'T$ value reflects the ground state spin value without the possible complications of the Zeeman effect from an applied dc field. The value expected for an $S = {}^{17}/_{2}$ state with $g = 2$ is 40.38 cm^3 K mol^{-1}, as mentioned earlier; thus, the observed value of ~40 cm^3 K mol^{-1} confirms an $S = {}^{17}/_{2}$ ground state with a g value slightly less than 2, in agreement with the dc magnetization fit. The expected values of $\chi_M'T$ (with $g = 2$) for $S = {}^{15}/_{2}$ and ${}^{19}/_{2}$ states are 31.88 and 49.88 cm^3 K mol^{-1}, respectively. In addition, the essentially constant $\chi_M'T$ value in this temperature range suggests the excited states are not too close to the ground state.

To confirm whether **3** is a SMM, studies were carried out on a single crystal down to 0.04 K, using a micro-SQUID instrument.[35] Shown in Figure 7 are the results of magnetization (M) versus applied dc field at a 0.002 T/s sweep rate. A hysteresis loop was observed, whose coercivity was strongly temperature-dependent (Figure 7, top) and time-dependent (Figure 7, bottom), increasing with decreasing temperature and increasing field sweep rate, as expected for the super-

(33) (a) Boyd, P. D. W.; Martin, R. L. *J. Chem. Soc., Dalton Trans*. **1979**, 92. (b) Gerloch, M.; McMeeking, R. F. *J. Chem. Soc., Dalton Trans*. **1975**, 2443.

(34) Davidson, E. R. *MAGNET*; Indiana University: Bloomington, IN.

(35) Wernsdorfer, W. *Adv. Chem. Phys.* **2001**, *118*, 99.

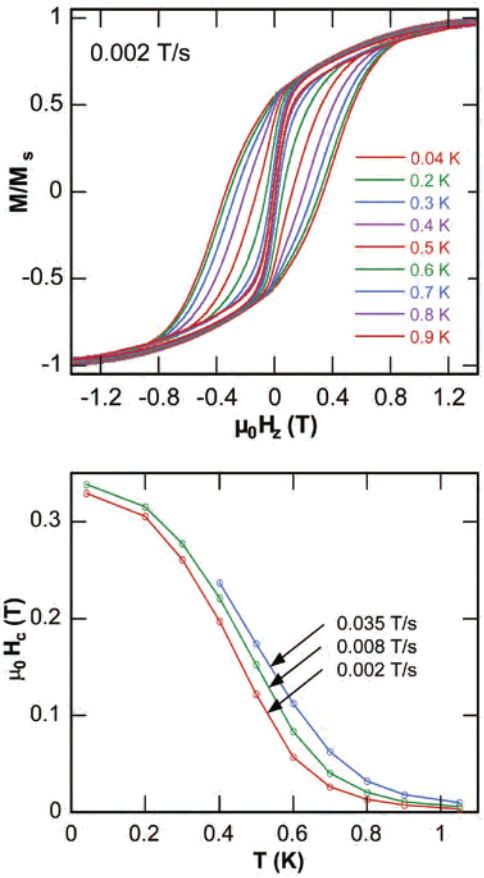

Figure 7. (top) Magnetization vs dc field hysteresis loops for a single crystal of **3** at the indicated temperatures and at a field sweep rate of 0.002 T/s. (bottom) Coercive field vs temperature plots at the indicated field sweep rates.

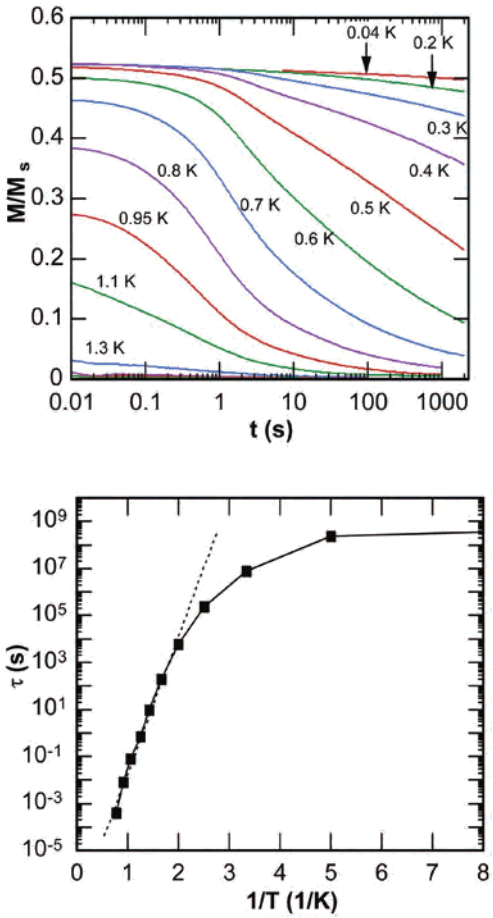

Figure 8. (top) Magnetization decay plots for a single crystal of **3** at the indicated temperatures. (bottom) Arrhenius plot constructed using the data from the decay plots. The dashed line is the best fit of the experimental data above 0.5 K to the Arrhenius equation. See the text for the fitting parameters.

paramagnetic-like behavior of a SMM. The blocking temperature (T_B) is ~1.1 K (Figure 7, bottom). Above this temperature, there is no hysteresis; that is, the spin relaxes faster to equilibrium than the time scale of the hysteresis loop measurement. The hysteresis loops for **3** do not show the steplike features indicative of quantum tunneling of magnetization (QTM) between the energy states of the molecule, contrary to what is observed for several SMMs.[3,36] This absence of well defined QTM steps can be rationalized as being primarily due to a distribution of molecular environments and thus a distribution of magnetization relaxation barriers (i.e., D values). Thus, broadening effects will smear the steps out. This is, in fact, consistent with the distribution of molecular environments resulting from the disordered perchlorate and solvent molecules observed in the crystal structure. In addition, weak intermolecular interactions (exchange and/or dipolar) will also contribute to broadening of steps. Similar hysteresis loops showing no QTM steps are a common feature of larger SMMs, where inefficient packing of the molecules in the crystal results in areas of disordered solvents, counterions, and/or carboxylate ligands. Examples include $[Mn_{18}O_{14}(O_2CMe)_{18}(hep)_4(hepH)_2(H_2O)_2](ClO_4)_2$,[8] a $[Mn_{26}]$ complex with fluoride ions,[9] and $[Mn_{30}O_{24}(OH)_8(O_2CCH_2Bu^t)_{32}(H_2O)_2(MeNO_2)_4]$.[10] In some cases, such as for the $[Mn_{18}]^{2+}$ complex mentioned, the presence of QTM could be confirmed by alternative types of measurement.[8]

Determination of the (mean) effective barrier to magnetization relaxation was accomplished using dc magnetization decay data. The magnetization of the molecules in the crystal was first saturated in one direction by application of a large dc field at 5 K, the temperature was then lowered to a chosen value in the 0.04−2 K range, the field was switched off, and the magnetization of the sample was monitored with time. The results are presented in Figure 8 (top). The decay data at each temperature were analyzed to produce a relaxation rate ($1/\tau$, where τ is the relaxation time). The combined rate versus T data were used to construct the Arrhenius plot in Figure 8 (bottom), on the basis of the Arrhenius equation of eq 3, where $1/\tau_0$ is the pre-exponential factor, U_{eff} is the mean effective barrier to relaxation, and k is the Boltzmann constant.

$$1/\tau = (1/\tau_0)\exp(-U_{eff}/kT) \qquad (3)$$

(36) (a) Friedman, J. R.; Sarachik, M. P.; Tejada, J.; Maciejewski, J.; Ziolo, R. *J. Appl. Phys.* **1996**, *79*, 6031. (b) Sangregorio, C.; Ohm, T.; Paulsen, C.; Sessoli, R.; Gatteschi, D. *Phys. Rev. Lett.* **1997**, *78*, 4645. (c) Aubin, S. M. J.; Dilley, N. R.; Pardi, L.; Krzystek, J.; Wemple, M. W.; Brunel, L.-C.; Maple, M. B.; Christou, G.; Hendrickson, D. N. *J. Am. Chem. Soc.* **1998**, *120*, 4991. (d) Brechin, E. K.; Soler, M.; Christou, G.; Helliwell, M.; Teat, S. J.; Wernsdorfer, W. *Chem. Commun.* **2003**, *11*, 1276.

The fit of the thermally activated region above ~0.5 K gave $\tau_0 = 4.2 \times 10^{-8}$ s and $U_{eff} = 13.2$ K. The fitting is shown as a dashed line in Figure 8 (bottom). The obtained barrier to relaxation thus is small, which is consistent with the small value of *D* suggested by the reduced magnetization fits and the observation of hysteresis only at very low temperatures. Nevertheless, complex **3** is a new member of the still small but growing family of single-molecule magnets.

Below ~0.2 K, the relaxation rate becomes temperature-independent, and this is characteristic of ground state tunneling between the lowest energy $M_S = \pm^{17}/_2$ levels of the $S = {}^{17}/_2$ spin manifold. Note also that the coercivity of the hysteresis loops of Figure 7 becomes essentially temperature-independent below ~0.2 K, and this is also a reflection of the relaxation occurring only by ground state tunneling. Although tunneling in the absence of an applied transverse field should not in theory occur for a half-integer spin system, transverse components of dipolar and exchange fields and/or nuclear spin fields from the ^{55}Mn nuclei ($I = {}^5/_2$, ~100% natural abundance) are believed to be the reason that tunneling has nevertheless always been seen to date in half-integer spin systems.[1,13]

Conclusions

The reaction of preformed Mn_3 and Mn_{10} clusters has afforded the new complex $[Mn_{21}O_{14}(OH)_2(O_2CMe)_{16}(hmp)_8(pic)_2(py)(H_2O)](ClO_4)_4$ (**3**), not available from simpler starting materials. This is a new structural type in the growing family of high nuclearity Mn/O complexes. The Mn_{21} cation of **3** is mixed-valent and has an unusual and low symmetry structure. Both dc and ac data indicate **3** to have an $S = {}^{17}/_2$ ground state and a small absolute value of the axial anisotropy parameter, *D*. The latter is consistent with the relatively random orientations of the Mn(III) Jahn−Teller elongation axes, which represent the source of the single-ion anisotropy at each Mn(III) atom, and the projections of which onto the molecular easy axis determine the overall molecular anisotropy. As a result, the overall barrier is relatively low. Thus, this complex provides another reminder of the importance of a complex to have both a significant ground state *S* value and a significant anisotropy of the easy-axis type before it can function as a SMM. The $S = {}^{17}/_2$ ground state of **3** is one of the largest ever observed, but a low value of *D* gives only a small barrier to relaxation. Nevertheless, another important datum point has been obtained for the increasing understanding of this interesting magnetic phenomenon of single-molecule magnetism.

Acknowledgment. We thank the National Science Foundation for financial support.

Supporting Information Available: X-ray crystallographic files in CIF format for complex **3**·7MeCN. This material is available free of charge via the Internet at http://pubs.acs.org.

IC0353864